

IDET: Iterative Difference-Enhanced Transformers for High-Quality Change Detection

Rui Huang¹, Ruofei Wang¹, Qing Guo^{2,*}, Yuxiang Zhang¹, Wei Fan¹

¹Civil Aviation University of China

²Nanyang Technological University

Abstract

Change detection (CD) aims to detect change regions within an image pair captured at different times, playing a significant role for diverse real-world applications. Nevertheless, most of existing works focus on designing advanced network architectures to map the feature difference to the final change map while ignoring the influence of the quality of the feature difference. In this paper, we study the CD from a new perspective, *i.e.*, how to optimize the feature difference to highlight changes and suppress unchanged regions, and propose a novel module denoted as *iterative difference-enhanced transformers (IDET)*. IDET contains three transformers: two transformers for extracting the long-range information of the two images and one transformer for enhancing the feature difference. In contrast to the previous transformers, the third transformer takes the outputs of the first two transformers to guide the enhancement of the feature difference iteratively. To achieve more effective refinement, we further propose the *multi-scale IDET-based change detection* that uses multi-scale representations of the images for multiple feature difference refinements and proposes a coarse-to-fine fusion strategy to combine all refinements. Our final CD method outperforms seven state-of-the-art methods on six large-scale datasets under diverse application scenarios, which demonstrates the importance of feature difference enhancements and the effectiveness of IDET.

Introduction

Change detection (CD) aims to detect change areas caused by object variations (*e.g.*, new objects appear in the scene) from an image pair captured at different times, which has wide applications in urban development (Buch, Velastin, and Orwell 2011), disaster assessment (Brunner, Bruzzone, and Lemoine 2010), resource monitoring, and utilization (Gong et al. 2015; Khan et al. 2017; Mou, Bruzzone, and Zhu 2018), abandoned object detection (Lin et al. 2015), illegally parked vehicles (Albiol et al. 2011) and military (Liu, Chen, and Kubota 2013; Liang et al. 2017). Change detection is still challenging since the two images might be captured at different angles and illuminations, and the scenes might have unknown changes in the background. As the case shown in Fig. 1 (b), the color of the sky and the intensity on buildings

vary dramatically within the two images, which, however, should not be identified as changes.

A straightforward idea is to calculate the differences between the features of the two images and map the feature difference to the final change map (Huang et al. 2020; Zhang et al. 2021). The features and feature differences are desired to conquer the environment variation and position misalignment. A representative work (Huang et al. 2020) proposes cross-encoded features to calculate the feature differences of an image pair and generate a change map. FPIN (Huang et al. 2021) uses a complex feature extraction network (*i.e.*, fluid pyramid integration network (Zhao et al. 2019)) to improve the CD accuracy by improving feature representational capability. Another work (Zhang et al. 2021) proposes position-correlated attention, channel-correlated attention, and change difference modules to capture the correlation of the two images. The above state-of-the-art (SOTA) methods focus on designing advanced network architectures to map the feature difference to the final change map. Although achieving impressive detection accuracy, these methods ignore the influence of the quality of the feature difference. Intuitively, if the feature difference could clearly highlight the main changes while suppressing unchanged regions, we are able to achieve high-quality change maps more easily. As the cases shown in Fig. 1, when the feature difference (*i.e.*, **D**) is corrupted (*e.g.*, noisy feature difference in Fig. 1 (b) and (c)), the detection results decrease significantly. Note that, the quality of feature difference may be affected by diverse environment variations like the light or weather changes.

To fill this gap, we study CD from a new angle, *i.e.*, how to optimize the feature difference to highlight main changes and suppress unchanged regions, and propose a novel module denoted as *iterative difference-enhanced transformers (IDET)*. IDET contains three transformers, the first two transformers are to extract the global information of the two input images while the third transformer is to enhance the feature differences. Note that, the third transformer is different from existing transformers, taking the outputs of the first two transformers to guide the feature difference refinement iteratively. Then, we fuse these refinements for high-quality detection via a coarse-to-fine method. Overall, our contributions can be summarized as follows:

- We build a basic feature difference-based change detection method and study the influence of feature difference

*The corresponding author: qing.guo@ntu.edu.sg.
Copyright © 2022, All rights reserved.

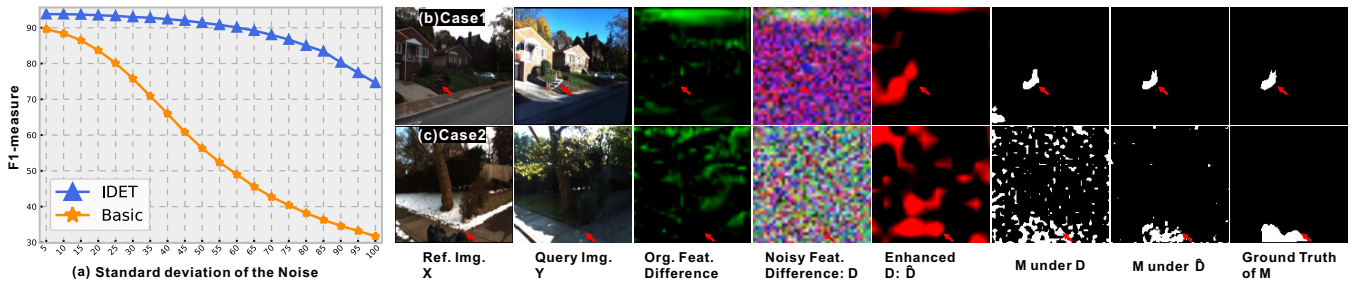


Figure 1: (a) Evaluation results on the VL-CMU-CD dataset (Alcantarilla et al. 2018) by adding noise with different severities to the feature difference D . (b) and (c) display two cases including the original feature difference, noisy feature difference D , enhanced feature difference \hat{D} , the detection results M under D and \hat{D} , and the ground truth, respectively. The main changes are highlighted via red arrows.

quality on the detection accuracy by adding random noise with different severities. The analysis infers that the feature difference quality is critical to high-quality detection.

- We propose a novel module, *i.e.*, iterative difference-enhanced transformer (IDET), to refine the feature difference by extracting the long-range information within inputs as the guidance.
- We conduct extensive experiments on six datasets covering wide range scenarios, image resolutions, and change ratios. Our method outperforms seven state-of-the-art methods.

Related Work

Change detection methods. According to different applications, CD methods can be divided into two types: CD for common scenarios and remote sensing. Both types retrieve change information from an image pair. The main differences stem from the image resolutions and the size of change regions.

CD methods for common scenarios (Guo et al. 2018; Huang et al. 2021) use images captured by consumer cameras and the results are affected by camera pose misalignment and illumination difference easily. The input images for remote sensing CD methods contain high-resolution remote sensing images (Zhang and Shi 2020; Chen et al. 2020), hyper spectral images (Wang et al. 2018), SAR images (Wang et al. 2020), *etc.* However, the changes are usually subtle. Early works have demonstrated the effectiveness of principal component analysis (PCA) (Li and Yeh 1998) and change vector analysis (CVA) (Malila 1980) for CD. With the development of deep neural networks, recent methods also adopt deep neural networks as the mainstream solution. FPIN (Huang et al. 2021) employs different fluid pyramid integration networks to fuse multi-level features. Dual correlation attention modules are utilized to refine the change features on same scale (Zhang et al. 2021).

However, these works mainly focus on designing novel deep architectures. In contrast, we focus on a new problem, *i.e.*, the influence of feature difference quality. With extensive study, we propose a feature difference enhancement or refinement method, which outperforms SOTA methods on

diverse applications including the common and remote sensing scenarios.

Transformer for vision tasks. The transformer has been widely used in most natural language processing (NLP) tasks for its long-range dependency since it was proposed in (Vaswani et al. 2017). Recently, the transformer has shown promising performance in computer vision tasks, such as image classification (Dosovitskiy et al. 2020; Sun et al. 2021; Li et al. 2021), object detection (Carion et al. 2020; Touvron et al. 2021; Zhu et al. 2020), semantic segmentation (Zheng et al. 2021; Liu et al. 2021; Dong et al. 2021; Xie et al. 2021), and crowd counting (Liang et al. 2021; Sun et al. 2021). The excellent performance of transformer models inspires us to study its application in CD. Till now, there are few works using the transformer for CD task. BiT (Hao Chen and Shi 2021) agrees that the transformer encoder can model the semantic information of change objects to refine the coarse change maps predicted by the decoder. However, it is difficult to learn the semantic tokens when the changed objects are small and diverse. ChangeFormer (Bandara and Patel 2022) is composed of a series hierarchically structured transformer encoders for extracting the long-range features to generate change masks. Due to the low resolutions of its encoders, which can not capture the detailed changes at the boundary.

In contrast to BiT (Hao Chen and Shi 2021) and ChangeFormer (Bandara and Patel 2022), our work has totally different objective and architecture. Specifically, the proposed module contains three transformers with a novel designed transformer for the effective feature difference refinement.

Feature Difference-based CD and Motivation

In this section, we first introduce, a lightweight convolutional neural network, the basic feature difference-based CD model and then analyze the issues from the viewpoint of the feature difference quality.

Feature Difference-based CD

Given a reference image X and a query image Y , a change detector $\phi(\cdot)$ takes the two images as the input and predicts a change map M that indicates changing regions between the two images, which are caused by object variations (*e.g.*, new objects appearing in the scene) instead of the environment

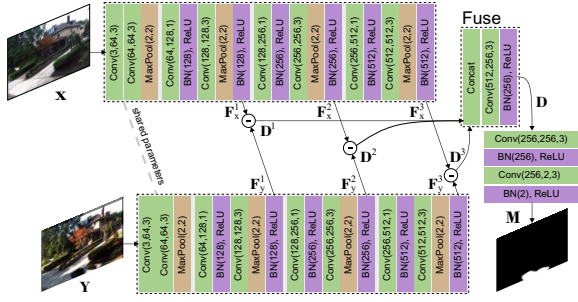


Figure 2: Architecture of feature difference-based CD.

changes (e.g., light variations). We can represent the whole process as $M = \phi(X, Y)$. The main challenge is how to distinguish the object changes from environment variations. Previous works calculate the difference between the features of X and Y explicitly and map it to the final change mask, which is robust to diverse environment variations (Huang et al. 2020). We follow the feature difference solution and build the *basic change detection method* via a CNN. Specifically, we feed X or Y to the CNN and get a series of features $\{F_x^l \text{ or } F_y^l\}_{l=1}^L$. Then, we can calculate the feature difference at each layer l and fuse them by a convolution layer

$$D = \text{Fuse}(\{D^l\}_{l=1}^L, \forall l, D^l = |F_x^l - F_y^l|), \quad (1)$$

where the feature difference D can be fed to other two convolution layers to predict the final change map M . We present all architecture details in Fig. 2. Previous works mainly focus on designing more advanced architecture to replace the basic CNN (Zhang et al. 2020). In contrast, we focus on the influence of the quality of D , which is not explored yet.

Analysis and Motivation

Based on Fig. 2, we study the importance of the quality of D to the final change map. Given an image pair from VL-CMU-CD dataset (Alcantarilla et al. 2018) (e.g., Fig. 1 (b) and (c)), we feed them to Eq. (1) and get the original feature difference denoted as D_0 . Then, we add random noise to the unchanged regions of D_0 to simulate the feature difference with diverse qualities. Specifically, according to the ground truth of the change regions, we first calculate the averages of feature difference values inside and outside change regions, which are denoted as d_0^{inside} and d_0^{outside} , respectively. Then, we set a zero-mean random noise with standard deviation as $\alpha |d_0^{\text{inside}} - d_0^{\text{outside}}|$ and add the noise to the unchanged regions in D_0 to get a degraded version denoted as D . We can conduct this process for all examples with the α from 5 to 100 with the interval of 5. Then, for each α , we can evaluate the detection results via the F1-measure. According to the dark orange stars in Fig. 1 (a), we see that the basic CD method is very sensitive to the quality of the feature difference. Clearly, as the noise becomes larger, the F1 value decreases significantly. We have similar conclusion on the visualization results in Fig. 1: the low-quality feature difference leads to incorrect detection.

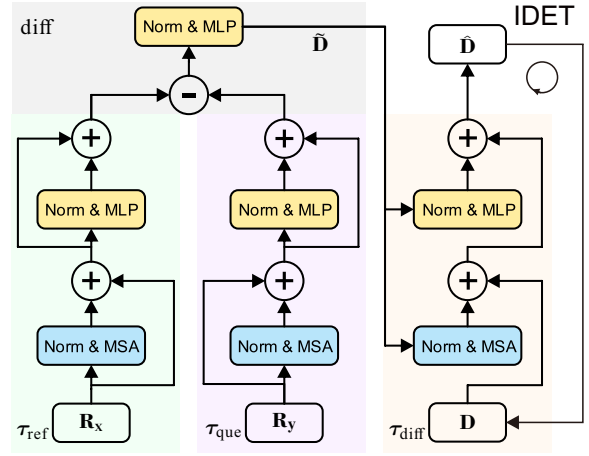


Figure 3: Architecture of Iterative Difference-enhanced Transformers (IDET).

Feature Difference Enhancement-based CD Problem Definition and Challenges

Due to the importance of feature difference quality, we formulate the feature difference enhancement as a novel task: given the representations of X and Y (i.e., R_x and R_y) and an initialized feature difference D , our goal is to refine D and get a better difference denoted as \hat{D} where the object changes are highlighted and other distractions are suppressed.

The feature difference enhancement is a non-trivial task since pixel changes between X and Y stem from the object and environment changes and it is difficult to distinguish the changes from each other. To achieve this refinement, a feature difference enhancement method should first understand the whole scene in both reference and query images and know which regions are caused by object changes. Moreover, the extracted discriminative information should be effectively embedded into the initial feature difference D to guide the refinement.

Iterative Difference-enhanced Transformers (IDET)

Overview. We employ the transformer to achieve the feature difference enhancement due to the impressive improvements of transformer-based methods in diverse vision tasks (Li et al. 2021; Xie et al. 2021). Note that, the transformer is able to capture the long-term dependency of the whole inputs, which meets the requirements of the feature difference enhancement. Nevertheless, how to adapt such an advanced technique to the new task is not clear. To this end, we propose the *iterative difference-enhanced transformers (IDET)* for feature difference enhancement.

IDET contains three transformers, i.e., reference transformer $\tau_{\text{ref}}(\cdot)$, query transformer $\tau_{\text{que}}(\cdot)$, and difference refinement transformer $\tau_{\text{diff}}(\cdot)$. The whole process of IDET is shown in Fig. 3 and can be formulated as:

$$\hat{D} = \tau_{\text{diff}}(D, \tilde{D}), \text{ with } \tilde{D} = \text{diff}(\tau_{\text{ref}}(R_x), \tau_{\text{que}}(R_y)), \quad (2)$$

where the transformers $\tau_{\text{ref}}(\cdot)$ and $\tau_{\text{que}}(\cdot)$ are employed to extract the long-range information in X and Y , respectively,

while the function $\text{diff}(\tau_{\text{ref}}(\mathbf{R}_x), \tau_{\text{que}}(\mathbf{R}_y))$ is

$$\begin{aligned} \tilde{\mathbf{D}} &= \text{diff}(\tau_{\text{ref}}(\mathbf{R}_x), \tau_{\text{que}}(\mathbf{R}_y)) \\ &= \text{MLP}(\text{Norm}(|\tau_{\text{ref}}(\mathbf{R}_x) - \tau_{\text{que}}(\mathbf{R}_y)|)). \end{aligned} \quad (3)$$

It aims to generate difference information (*i.e.*, $\tilde{\mathbf{D}}$) from the two long-range features (*i.e.*, $\tau_{\text{ref}}(\mathbf{R}_x)$ and $\tau_{\text{que}}(\mathbf{R}_y)$) through a multilayer perceptron (MLP) and a layer norm (Norm). Finally, the $\tilde{\mathbf{D}}$ is fed to the difference refinement transformer (*i.e.*, $\tau_{\text{diff}}(\cdot)$) to guide the updating of the initial \mathbf{D} . *Moreover, we can make the output $\tilde{\mathbf{D}}$ as the initial feature difference and refine it again and again. As a result, the method becomes iterative.* We show the whole architecture in Fig. 3 and detail them in the following subsections.

Architectures of $\tau_{\text{ref}}(\cdot)$ and $\tau_{\text{que}}(\cdot)$. We eliminate the position token and class token in the model designation because we don't use the patch embedding and ignore the object labels.

The whole process can be formulated as

$$\begin{aligned} \tau_*(\mathbf{R}_*) &= \text{MLP}(\text{Norm}(\mathbf{Z})) + \mathbf{Z}, \text{ with} \\ \mathbf{Z} &= \text{MSA}(\text{Norm}(\mathbf{R}_*)) + \mathbf{R}_*, \end{aligned} \quad (4)$$

where $\text{MSA}(\cdot)$ is the efficient multi-head self-attention introduced in (Xie et al. 2021).

Architecture of $\tau_{\text{diff}}(\cdot)$. In contrast to the above transformers, $\tau_{\text{diff}}(\cdot)$ is to use the difference information $\tilde{\mathbf{D}}$ obtained by Eq. (3) to guide the refinement of the initial \mathbf{D} . To this end, we modify the Eq. (4) by

$$\begin{aligned} \tau_{\text{diff}}(\mathbf{D}, \tilde{\mathbf{D}}) &= \text{MLP}(\text{Norm}(\tilde{\mathbf{D}})) + \mathbf{Z}, \text{ with} \\ \mathbf{Z} &= \text{MSA}(\text{Norm}(\tilde{\mathbf{D}})) + \mathbf{D}. \end{aligned} \quad (5)$$

The intuitive idea is to use MSA and MLP to extract the long-term information in $\tilde{\mathbf{D}}$ and embed it to update the initial \mathbf{D} .

Multi-scale IDET-based CD

With the proposed IDET, we are able to update the basic feature difference-based CD introduced in the above. The key problem is how to select the representations (*i.e.*, \mathbf{R}_x and \mathbf{R}_y in Eq. (2)) to refine the feature difference \mathbf{D} in Eq. (1) and how to fuse refined results from different representations. Here, we propose to use UNet (Ronneberger, Fischer, and Brox 2015) to extract multi-scale convolutional features as the representations and can get a refined feature difference for each scale, and then design a coarse-to-fine fusion method to combine multi-scale results. Specifically, given a UNet containing an encoder and a decoder, we feed \mathbf{X} and \mathbf{Y} to the network, respectively, and get multi-scale representations from all the layers of the decoder, which are denoted as $\{\mathbf{R}_x^l\}^L$ and $\{\mathbf{R}_y^l\}^L$ where L denotes the number of scales. Note that, given \mathbf{R}_x^l and \mathbf{R}_y^l , we still cannot refine \mathbf{D} through the IDET directly since $\tilde{\mathbf{D}}$ from Eq. (1) has smaller resolution than \mathbf{R}_x^l and \mathbf{R}_y^l . To use IDET at the scale l , we upsample \mathbf{D} to the size of \mathbf{R}_x^l and \mathbf{R}_y^l and get a refined result $\hat{\mathbf{D}}^l$. For all scales, we have $\{\hat{\mathbf{D}}^l\}_{l=1}^L$ and fuse them via

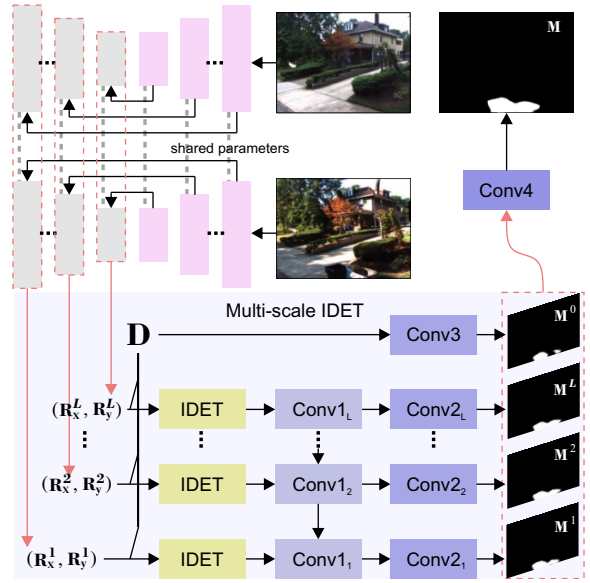


Figure 4: Multi-scale IDET-based CD.

a coarse-to-fine strategy, *i.e.*,

$$\hat{\mathbf{D}}^l = \text{Conv1}_l([\hat{\mathbf{D}}^l, \hat{\mathbf{D}}^{(l-1)}]), \text{ with } l = 1, \dots, L, \quad (6)$$

where $[\cdot]$ denotes the concatenation operation and $\hat{\mathbf{D}}^0 = \emptyset$. For $\hat{\mathbf{D}}^l$ and the initial \mathbf{D} , we use a convolution layer to extract a change map

$$\mathbf{M}^l = \text{Conv2}_l(\hat{\mathbf{D}}^l), \text{ and } \mathbf{M}^0 = \text{Conv3}(\mathbf{D}). \quad (7)$$

Then, the final output is obtained via $\mathbf{M} = \text{Conv4}([\mathbf{M}^0, \dots, \mathbf{M}^L])$.

Implementation Details

Architecture of UNet. We follow the UNet implementation of (Huang et al. 2020). It has five squeeze modules to extract abstract features by reducing the spatial resolution and five expanded modules to restore the resolution of the features by incorporating high-resolution and low-level features from squeeze modules.

Setups of Conv* for fusion. $\text{Conv1}_*(\cdot)$ contains three modules, each of which has a convolutional layer and a ReLU layer. The first convolutional layer is responsible for reducing the channel number to half of the channel number of the input feature. The second convolutional layer has same input and output channel number to further refine the feature. The third convolutional layer produces feature with a given output channel number. The filter size in these convolutional layers are 3×3 . $\text{Conv2}_*(\cdot)$ is a convolutional layer with filters of size with $N \times 3 \times 3 \times 2$, where N represents the input channel number. $\text{Conv3}(\cdot)$ is used to generate change map \mathbf{M}^0 from the feature difference \mathbf{D} . $\text{Conv4}(\cdot)$ consists of $12 \times 3 \times 3 \times 2$ convolutional filters to generate final change map \mathbf{M} .

Loss functions. Given a predicted change map \mathbf{M}^* and the ground truth, we can calculate the cross-entropy loss denoted as $\mathcal{L}_{\mathbf{M}^*}$. We employ the cross-entropy loss on all the

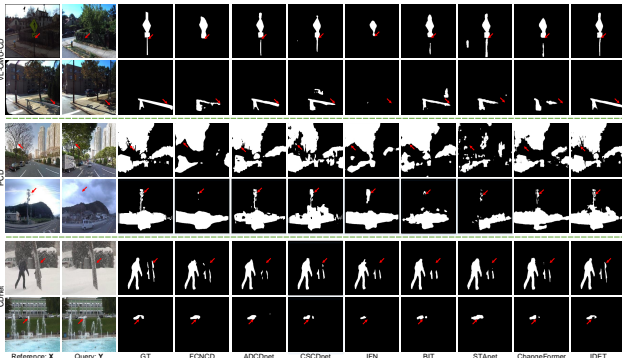


Figure 5: Detection results of different CD methods on VL-CMU-CD (Alcantarilla et al. 2018), PCD (Sakurada and Okatani 2015) and CDnet (Goyette et al. 2012).

predicted change maps of M^0, \dots, M^L and M , and get a total loss:

$$\mathcal{L} = \sum_{l=1}^L \mathcal{L}_{M^l} + \mathcal{L}_M. \quad (8)$$

Training parameters. Our model is implemented on PyTorch (Paszke et al. 2017) and trained with a single NVIDIA Geforce 2080Ti GPU. The basic learning rate is set to $1e-3$. We set the batch size to 4. The parameters are updated by Adam algorithm with a momentum of 0.9 and weight decay of 0.999. Note that we use the same training parameters for all six datasets. Following (Huang et al. 2020) and (Chen and Shi 2020), we train all CD methods with 20 and 200 epochs for common scene datasets and remote sensing datasets, respectively.

Experiments

Setup

Baselines. We compare the proposed method with seven CD methods, i.e., FCNCD (Long, Shelhamer, and Darrell 2015), ADCDnet (Huang et al. 2020), CSCDnet (Sakurada, Shibuya, and Wang 2020), BIT (Hao Chen and Shi 2021), IFN (Zhang et al. 2020), STAnet (Chen and Shi 2020) and ChangeFormer (Bandara and Patel 2022). All compared methods are implemented with Pytorch and trained on the same training sets.

Datasets. We conduct experiments on three common-sense CD datasets, i.e., VL-CMU-CD (Alcantarilla et al. 2018), PCD (Sakurada and Okatani 2015) and CDnet (Goyette et al. 2012), and three remote sensing CD datasets, i.e., LEVIR-CD (Chen and Shi 2020), CDD (Shunping et al. 2019) and AICD (Bourdis, Marraud, and Sahbi 2011). For VL-CMU-CD (Alcantarilla et al. 2018), we randomly select 80% image pairs for training and 20% for testing. The training images are augmented by randomly clipping and flipping. For PCD (Sakurada and Okatani 2015), we crop the image with a size of 224×224 , and partition the training and testing set with a ratio of 8:2. The training images are flipped to increase the number of training images. For CDnet (Goyette et al. 2012), we use the training and testing dataset as proposed (Huang et al. 2020). For

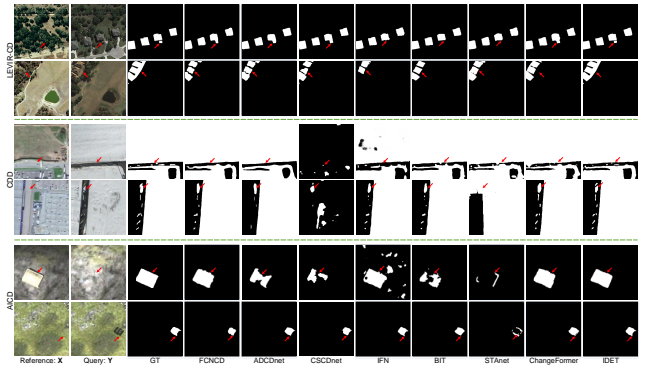


Figure 6: Detection results of different CD methods on LEVIR-CD (Chen and Shi 2020), CDD (Shunping et al. 2019) and AICD (Bourdis, Marraud, and Sahbi 2011).

LEVIR-CD (Chen and Shi 2020), we crop images into small patches of size 256×256 without overlapping and augment training images with rotation and color transformation. Finally, we obtain 15835 and 4675 image pairs for training and testing, respectively. For CDD (Shunping et al. 2019), we crop and rotate the original images to generate 10000 training and 3000 testing image pairs as proposed in (Shunping et al. 2019). For AICD (Bourdis, Marraud, and Sahbi 2011), we crop image pairs randomly and augment the training images by rotation and color vibration.

Evaluation metrics. Following (Hao Chen and Shi 2021), we use precision (P), recall (R), F1-measure (F1), over- all accuracy (OA) and intersection over union (IoU) to evaluate different CD methods.

Comparison Result

Results of common sense datasets. Fig. 5 shows the typical detection results of different CD methods on VL-CMU-CD, PCD, and CDnet datasets. Compared with IFN (Zhang et al. 2020), BIT (Hao Chen and Shi 2021), STAnet (Chen and Shi 2020) and ChangeFormer (Bandara and Patel 2022) that is designed for remote sensing, FCNCD (Long, Shelhamer, and Darrell 2015), ADCDnet (Huang et al. 2020), CSCDnet (Sakurada, Shibuya, and Wang 2020) and IDET show better CD results for common scene CD. FCNCD (Long, Shelhamer, and Darrell 2015) only captures the main parts of changes, which loses the details of the changes as shown in the 1st to 4th rows of Fig. 5. IFN (Zhang et al. 2020) also loses the detailed information of changes, even loses the all change object in the 2nd row of Fig. 5. BIT (Hao Chen and Shi 2021) can be easily affected by shadows and background clusters, which results in false detection in the 2nd and 6th rows of Fig. 5. Similarly, the transformer based ChangeFormer (Bandara and Patel 2022) also has this shortage. STAnet (Chen and Shi 2020) generates incomplete CD results as shown in 4th and 5th rows of Fig. 5. Among the compared methods, ADCDnet (Huang et al. 2020) has the moderate CD results on all three CD datasets. However, we can find that the results of IDET are more complete and have more details as shown in the last column of Fig. 5.

Table 1 shows the quantitative comparison of different CD methods on VL-CMU-CD, PCD and CDnet dataset. On VL-

Table 1: Quantitative comparison of different CD methods on VL-CMU-CD (Alcantarilla et al. 2018), PCD (Sakurada and Okatani 2015) and CDnet (Goyette et al. 2012). The **bold** is the best.

Method	VL-CMU-CD					PCD					CDnet				
	P	R	F1	OA	IoU	P	R	F1	OA	IoU	P	R	F1	OA	IoU
FCNCD	84.2	84.3	84.2	98.4	72.9	68.7	61.7	65.0	94.1	48.0	82.9	88.3	85.5	99.2	76.0
ADCDnet	92.8	94.3	93.5	99.3	87.9	78.8	73.4	76.0	90.0	62.3	89.0	85.5	87.2	99.3	77.9
CSCDnet	89.2	91.1	90.1	98.7	82.1	66.0	72.6	69.1	83.7	51.9	93.9	82.3	87.7	99.0	78.4
IFN	93.1	75.9	83.6	98.1	71.4	69.5	75.7	72.5	87.2	57.7	93.1	80.0	86.1	98.9	75.3
BIT	90.5	87.6	89.0	98.8	80.6	77.7	57.3	66.0	85.4	50.1	95.4	81.9	88.1	99.1	78.9
STAnet	73.1	95.8	82.9	98.0	70.7	69.6	52.7	60.0	79.9	41.2	72.2	94.3	81.8	98.3	69.2
ChangeFormer	88.0	88.6	88.3	98.7	79.2	74.0	69.2	71.5	86.6	56.4	93.4	85.9	89.5	99.2	81.3
IDET (Ours)	93.5	94.5	94.0	99.4	88.7	74.2	77.9	76.0	88.8	61.9	90.8	94.1	92.4	99.7	86.2

Table 2: Quantitative comparison of different CD methods on LEVIR-CD (Chen and Shi 2020), CDD (Shunping et al. 2019) and AICD (Bourdis, Marraud, and Sahbi 2011). The **bold** is the best.

Method	LEVIR-CD					CDD					AICD				
	P	R	F1	OA	IoU	P	R	F1	OA	IoU	P	R	F1	OA	IoU
FCNCD	89.7	84.0	86.8	97.7	77.1	85.1	69.8	76.7	97.5	63.7	81.4	87.7	84.4	99.9	72.7
ADCDnet	90.4	81.8	85.9	97.4	75.4	92.5	78.8	85.1	98.5	75.1	85.0	99.0	91.5	99.9	84.2
CSCDnet	84.6	81.6	83.1	96.8	71.5	79.1	48.9	60.4	90.9	42.7	92.5	88.9	90.7	99.9	82.6
IFN	89.7	79.8	84.5	96.9	72.7	94.2	69.2	79.8	97.7	66.5	84.6	97.7	90.7	99.9	82.9
BIT	92.1	81.6	86.5	97.7	76.3	93.5	80.2	86.3	98.7	76.6	94.2	92.4	93.2	99.9	87.4
STAnet	84.8	69.9	76.6	95.3	61.8	71.6	69.6	70.6	95.0	54.6	46.0	35.6	40.1	99.4	22.4
ChangeFormer	90.7	85.5	88.0	98.0	79.0	89.2	73.0	80.3	98.0	68.0	82.7	98.3	89.8	99.9	81.5
IDET (Ours)	91.3	86.6	88.9	98.1	80.2	91.1	83.1	86.9	98.7	77.6	96.2	90.4	93.2	99.9	87.2

CMU-CD, almost all the criteria of IDET are better than other compared methods. Take the ADCDnet (Huang et al. 2020) for example, whose F1, OA and IoU are very close to IDET. Compared with the best remote sensing CD method BIT (Hao Chen and Shi 2021), IDET achieves 5.9%, 0.6% and 10.0% relative F1, OA and IoU improvements, respectively. On PCD dataset, there are only four CD methods, whose F1 values are higher than 70%. ADCDnet (Huang et al. 2020) shows the best performance than other CD methods. Compared with ADCDnet (Huang et al. 2020), the IoU of IDET are a bit lower than ADCDnet (Huang et al. 2020). On CDnet dataset, only the F1 value and IoU of IDET are higher than 90% and 85%, respectively. ChangeFormer (Bandara and Patel 2022) achieves the best CD performance than other compared methods. However, compared with ChangeFormer, IDET achieves 3.2%, 0.5% and 6.2% relative F1, OA and IoU improvements, respectively.

Results of remote sensing datasets. Fig. 6 shows typical detection results of different CD methods on LEVIR-CD, CDD and AICD datasets. Only FCNCD (Long, Shelhamer, and Darrell 2015), ADCDnet (Huang et al. 2020), CSCDnet () and ChangeFormer (Bandara and Patel 2022) detect the whole buildings but can not separate them in the 1st row of Fig. 6. Among the compared method, only IDET can detect the connected changes in the 2nd row of Fig. 6. CSCDnet (Sakurada, Shibuya, and Wang 2020) regards the vast majority of change areas in 3rd and 4th image pairs as the background. In the last two image pairs of Fig. 6, we also find that most of the compared methods are easily affected by overexposure. On the contrary, only IDET, FCNCD (Long, Shelhamer, and Darrell 2015) and ChangeFormer (Bandara and Patel 2022) can generate promising

CD results.

Table 2 shows the quantitative comparison of different CD methods on LEVIR-CD, CDD, and AICD. We can find that IDET has excellent performances on three remote sensing datasets in almost all criteria. Concretely, on LEVIR-CD, IDET achieves 1.0%, 0.1% and 1.5% relative F1, OA and IoU improvements than ChangeFormer (Bandara and Patel 2022), respectively. On CDD dataset, BIT (Hao Chen and Shi 2021) is the best CD method among the compared CD methods. The F1 and IoU of IDET are higher than BIT by 1.1% and 1.0%, respectively. On AICD, IDET has similar performance with BIT. Except FCNCD, STAnet and ChangeFormer, the F1 values and IoU of all other CD methods are higher than 90% and 82%, respectively.

Ablation Study

Novelty and differences to existing transformers. This work, for the first attempt, explore the critical role of the feature difference quality to the CD (See Fig. 1). The intuitive idea of IDET is to extract difference information for the representations of input images (*i.e.*, \mathbf{R}_x and \mathbf{R}_y) and use them to guide the refinement of the feature difference \mathbf{D} . To this end, we propose a novel transformer-based module that is different from previous ones (See Fig. 4). *First*, the whole IDET is novel and not a naive combination of three transformers. The transformers τ_{ref} and τ_{que} are to extract difference-related information in corresponding features (*i.e.*, \mathbf{R}_x and \mathbf{R}_y), and we design an extra function $\text{diff}(\cdot)$ to further refine the semantic differences. *Second*, the transformer τ_{diff} is a dynamic transformer and basically different from existing ones while it allows to borrowing the extra information (*i.e.*, $\tilde{\mathbf{D}}$) to guide the updating of the input

D dynamically (See Eq. (5)). *Third*, IDET allows the iterative optimization that benefits the detection accuracy significantly as demonstrated below.

Table 3: Ablation studies on multi scales and three transformers $\tau_{\text{ref}}(\cdot)$ & $\tau_{\text{que}}(\cdot)$, $\tau_{\text{diff}}(\cdot)$ (3rd transformer). We use the convolution block (consists of four convolution layers with batch normalization and ReLU) to replace the IDET and get a variant (*i.e.*, Multi-Scale-CNN-feat. diff. enhance.). We make this experiment on VL-CMU-CD. The **bold** is the best.

Methods	F1	OA	IoU
w/o feat. diff. enhance.	93.2	99.3	87.7
Multi-Scale-CNN-feat. diff. enhance	93.6	99.3	88.0
Multi-Scale.IDET-feat. diff. enhance. (Ours)	94.0	99.4	88.7
Naive-Multi-Scale.IDET-feat. diff. enhance.	93.8	99.3	88.4
Single-Scale.IDET-feat. diff. enhance.	93.7	99.3	88.2
Multi-Scale.IDET w/o $\tau_{\text{diff}}(\cdot)$	0.935	0.993	0.879
Single-Scale.IDET w/o $\tau_{\text{diff}}(\cdot)$	0.933	0.993	0.875
Multi-Scale.IDET w/o $\tau_{\text{ref}}(\cdot)$ & $\tau_{\text{que}}(\cdot)$	0.929	0.993	0.867
Single-Scale.IDET w/o $\tau_{\text{ref}}(\cdot)$ & $\tau_{\text{que}}(\cdot)$	0.924	0.992	0.860

Visualization of the feature difference enhancement.

We have visualized the importance of the feature difference enhancement in Fig. 1. Here, in Fig. 7, we further present three cases to compare the feature difference before and after enhancement (5th column vs. 7th column) and detection results with/without IDET. Clearly, IDET enhances the desired changes in the feature difference, leading to obvious advantages in final evaluations.

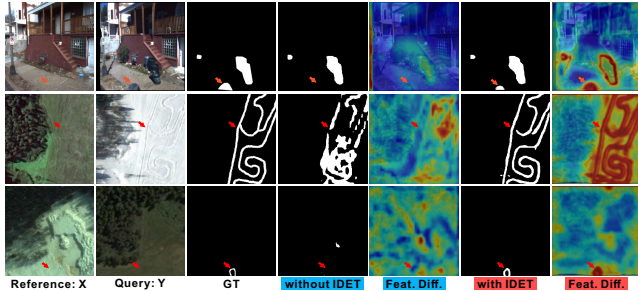


Figure 7: 3 cases with/without IDET. Main advantages are highlighted via red arrows.

Effectiveness of multiple losses with Focal loss and Cross entropy loss.

We add supervisions on all predicted change maps of M^0, \dots, M^L and M to train our model. To validate the effectiveness of using multiple supervision, we re-train our network only using single supervision on the final change map M with Cross entropy loss ($SS + CE$), multiple supervision with Focal loss ($MS + \mathcal{F}$), and multiple supervision with Cross entropy loss ($MS + CE$). As shown in Table. 4, we find that ❶ using multiple supervisions ($MS + CE$) achieves consistently F1, OA and IoU improvements over using single supervision ($SS + CE$); ❷ using Cross entropy loss ($MS + CE$) is more suitable for CD than using Focal loss ($MS + \mathcal{F}$).

Iteration of IDET. We set different iteration number (T) for IDET to study the influence of T . Table 5 shows the results of $T = 0$, $T = 1$ and $T = 2$ in IDET. Specifically, $T = 0$ means that the difference convolutional features are directly used for CD without iterative difference-enhanced transformers. We can find that except on CDnet,

Table 4: Results of our method with single supervision (SS) on the final layer and multiple supervision (MS), Focal loss (\mathcal{F}) and Cross entropy loss (CE). The **bold** is the best.

Dataset	$SS+CE$			$MS+\mathcal{F}$			$MS+CE$		
	F1	OA	IoU	F1	OA	IoU	F1	OA	IoU
VL-CMU-CD	91.6	99.3	87.3	91.6	99.2	84.6	94.0	99.4	88.7
PCD	75.0	88.9	60.3	70.1	88.1	54.4	76.0	88.8	61.9
CDnet	92.4	99.6	86.1	89.9	99.5	81.6	92.4	99.7	86.2
LEVIR-CD	87.8	97.8	78.3	82.5	97.0	70.3	88.9	98.1	80.2
CDD	78.0	97.6	64.3	70.8	97.1	55.1	85.4	98.5	75.2
AICD	88.5	99.9	79.4	88.8	99.9	80.4	91.4	99.3	82.5

using $T = 2$ in IDET achieves better performances on other datasets, which demonstrates that with limited GPU memory, using $T = 2$ in IDET improves the representational ability of the features.

On CDnet, using $T = 1$ results in the best F1, OA and IoU values than using $T = 0$ or 2. A possible reason is that the training and testing image pairs on CDnet are captured from same video, which results in a high correlation between the changes. Thus, a light-weighted model (*e.g.*, IDET with $T = 1$) can achieve better performances than the model with more iteration number in IDET.

Table 5: Results of different T in IDET. The **bold** is the best.

Dataset	F1			OA			IoU		
	$T=0$	$T=1$	$T=2$	$T=0$	$T=1$	$T=2$	$T=0$	$T=1$	$T=2$
VL-CMU-CD	93.2	93.6	94.0	99.3	93.8	99.4	87.7	88.4	88.7
PCD	71.2	73.8	76.0	88.3	89.5	88.8	58.5	61.7	61.9
CDnet	91.7	92.6	92.4	99.6	99.7	99.7	85.7	87.0	86.2
LEVIR-CD	87.0	82.9	88.9	98.0	97.3	98.1	79.3	74.0	80.2
CDD	80.0	82.9	85.4	98.1	98.5	98.5	69.4	73.4	78.2
AICD	89.5	90.5	91.4	99.9	99.9	99.9	81.4	82.8	84.4

Running time analysis. Table 6 shows the running time of different CD methods on a 320×320 image pair. The proposed IDET is faster than contemporary transformer based method ChangeFormer (Bandara and Patel 2022).

Table 6: Running time of different CD methods on a 320×320 image pair.

Method	FCNCD	ADCdnet	CSCdnet	IFN	BIT	STAnet	ChangeFormer	IDET
Time (ms)	14.5	21.9	79.0	21.6	39.9	28.8	85.9	68.1

Conclusion

In this paper, we identify an important factor (*i.e.*, the quality of feature difference) that affects the change detection accuracy significantly. To validate this, we built a basic feature difference-based change detection method and studied how the feature difference quality affects detection results. To fill this gap, we proposed a novel module (*i.e.*, iterative difference-enhanced transformers (IDET)) to refine the feature difference. Moreover, to achieve better refinement, we proposed the multi-scale IDET and used it for the final change detection. We have conducted extensive experiments and ablation studies to compare the proposed method with the state-of-the-art methods as well as different variations on six large-scale datasets covering a wide range of application scenarios, image resolutions, change ratios. Our method outperforms all baseline methods, which infers the importance of the feature difference quality.

References

- Albiol, A.; Sanchis, L.; Albiol, A.; and Mossi, J. M. 2011. Detection of parked vehicles using spatiotemporal maps. *IEEE Transactions on Intelligent Transportation Systems*, 12(4): 1277–1291.
- Alcantarilla, P. F.; Stent, S.; Ros, G.; Arroyo, R.; and Gherardi, R. 2018. Street-view change detection with deconvolutional networks. *Autonomous Robots*, 42(7): 1301–1322.
- Bandara, W. G. C.; and Patel, V. M. 2022. A transformer-based siamese network for change detection. *arXiv preprint arXiv:2201.01293*.
- Bourdis, N.; Marraud, D.; and Sahbi, H. 2011. Constrained optical flow for aerial image change detection. In *2011 IEEE International Geoscience and Remote Sensing Symposium*, 4176–4179. IEEE.
- Brunner, D.; Bruzzone, L.; and Lemoine, G. 2010. Change detection for earthquake damage assessment in built-up areas using very high resolution optical and SAR imagery. In *2010 IEEE International Geoscience and Remote Sensing Symposium*, 3210–3213. IEEE.
- Buch, N.; Velastin, S. A.; and Orwell, J. 2011. A review of computer vision techniques for the analysis of urban traffic. *IEEE Transactions on intelligent transportation systems*, 12(3): 920–939.
- Carion, N.; Massa, F.; Synnaeve, G.; Usunier, N.; Kirillov, A.; and Zagoruyko, S. 2020. End-to-end object detection with transformers. In *European Conference on Computer Vision*, 213–229. Springer.
- Chen, H.; and Shi, Z. 2020. A Spatial-Temporal Attention-Based Method and a New Dataset for Remote Sensing Image Change Detection. *Remote Sensing*, 12(10): 1662.
- Chen, J.; Yuan, Z.; Peng, J.; Chen, L.; Huang, H.; Zhu, J.; Lin, T.; and Li, H. 2020. DASNet: Dual attentive fully convolutional siamese networks for change detection of high resolution satellite images. *IEEE Journal of Selected Topics in Applied Earth Observations and Remote Sensing*.
- Dong, X.; Bao, J.; Chen, D.; Zhang, W.; Yu, N.; Yuan, L.; Chen, D.; and Guo, B. 2021. Cswin transformer: A general vision transformer backbone with cross-shaped windows. *arXiv preprint arXiv:2107.00652*.
- Dosovitskiy, A.; Beyer, L.; Kolesnikov, A.; Weissenborn, D.; Zhai, X.; Unterthiner, T.; Dehghani, M.; Minderer, M.; Heigold, G.; Gelly, S.; et al. 2020. An image is worth 16x16 words: Transformers for image recognition at scale. *arXiv preprint arXiv:2010.11929*.
- Gong, M.; Zhao, J.; Liu, J.; Miao, Q.; and Jiao, L. 2015. Change detection in synthetic aperture radar images based on deep neural networks. *IEEE transactions on neural networks and learning systems*, 27(1): 125–138.
- Goyette, N.; Jodoin, P.-M.; Porikli, F.; Konrad, J.; and Ishwar, P. 2012. Changedetection.net: A new change detection benchmark dataset. In *2012 IEEE computer society conference on computer vision and pattern recognition workshops*, 1–8. IEEE.
- Guo, E.; Fu, X.; Zhu, J.; Deng, M.; Liu, Y.; Zhu, Q.; and Li, H. 2018. Learning to measure change: Fully convolutional siamese metric networks for scene change detection. *arXiv preprint arXiv:1810.09111*.
- Hao Chen, Z. Q.; and Shi, Z. 2021. Remote Sensing Image Change Detection with Transformers. *IEEE Transactions on Geoscience and Remote Sensing*, 1–14.
- Huang, R.; Zhou, M.; Xing, Y.; Zou, Y.; and Fan, W. 2021. Change detection with various combinations of fluid pyramid integration networks. *Neurocomputing*, 437: 84–94.
- Huang, R.; Zhou, M.; Zhao, Q.; and Zou, Y. 2020. Change detection with absolute difference of multiscale deep features. *Neurocomputing*, 418: 102–113.
- Khan, S. H.; He, X.; Porikli, F.; and Bennamoun, M. 2017. Forest change detection in incomplete satellite images with deep neural networks. *IEEE Transactions on Geoscience and Remote Sensing*, 55(9): 5407–5423.
- Li, X.; and Yeh, A. 1998. Principal component analysis of stacked multi-temporal images for the monitoring of rapid urban expansion in the Pearl River Delta. *International Journal of Remote Sensing*, 19(8): 1501–1518.
- Li, Y.; Zhang, K.; Cao, J.; Timofte, R.; and Van Gool, L. 2021. Localvit: Bringing locality to vision transformers. *arXiv preprint arXiv:2104.05707*.
- Liang, D.; Chen, X.; Xu, W.; Zhou, Y.; and Bai, X. 2021. TransCrowd: Weakly-Supervised Crowd Counting with Transformer. *arXiv preprint arXiv:2104.09116*.
- Liang, D.; Kaneko, S.; Sun, H.; and Kang, B. 2017. Adaptive local spatial modeling for online change detection under abrupt dynamic background. In *2017 IEEE International Conference on Image Processing (ICIP)*, 2020–2024. IEEE.
- Lin, K.; Chen, S.-C.; Chen, C.-S.; Lin, D.-T.; and Hung, Y.-P. 2015. Abandoned object detection via temporal consistency modeling and back-tracing verification for visual surveillance. *IEEE Transactions on Information Forensics and Security*, 10(7): 1359–1370.
- Liu, H.; Chen, S.; and Kubota, N. 2013. Intelligent video systems and analytics: A survey. *IEEE Transactions on Industrial Informatics*, 9(3): 1222–1233.
- Liu, Z.; Lin, Y.; Cao, Y.; Hu, H.; Wei, Y.; Zhang, Z.; Lin, S.; and Guo, B. 2021. Swin transformer: Hierarchical vision transformer using shifted windows. *arXiv preprint arXiv:2103.14030*.
- Long, J.; Shelhamer, E.; and Darrell, T. 2015. Fully convolutional networks for semantic segmentation. In *Proceedings of the IEEE conference on computer vision and pattern recognition*, 3431–3440.
- Malila, W. A. 1980. Change vector analysis: an approach for detecting forest changes with Landsat. In *LARS symposia*, 385.
- Mou, L.; Bruzzone, L.; and Zhu, X. X. 2018. Learning spectral-spatial-temporal features via a recurrent convolutional neural network for change detection in multispectral imagery. *IEEE Transactions on Geoscience and Remote Sensing*, 57(2): 924–935.
- Paszke, A.; Gross, S.; Chintala, S.; Chanan, G.; Yang, E.; DeVito, Z.; Lin, Z.; Desmaison, A.; Antiga, L.; and Lerer, A. 2017. Automatic differentiation in pytorch.

- Ronneberger, O.; Fischer, P.; and Brox, T. 2015. U-net: Convolutional networks for biomedical image segmentation. In *International Conference on Medical image computing and computer-assisted intervention*, 234–241. Springer.
- Sakurada, K.; and Okatani, T. 2015. Change Detection from a Street Image Pair using CNN Features and Superpixel Segmentation. In *Proceedings of the British Machine Vision Conference (BMVC)*, 61.1–61.12. BMVA Press.
- Sakurada, K.; Shibuya, M.; and Wang, W. 2020. Weakly supervised silhouette-based semantic scene change detection. In *2020 IEEE International conference on robotics and automation (ICRA)*, 6861–6867. IEEE.
- Shunping; Ji; Shiqing; Wei; Meng; and Lu. 2019. Fully Convolutional Networks for Multisource Building Extraction From an Open Aerial and Satellite Imagery Data Set. *IEEE Transactions on Geoscience and Remote Sensing*, 57(1): 574–586.
- Sun, G.; Liu, Y.; Probst, T.; Paudel, D. P.; Popovic, N.; and Van Gool, L. 2021. Boosting Crowd Counting with Transformers. *arXiv preprint arXiv:2105.10926*.
- Touvron, H.; Cord, M.; Douze, M.; Massa, F.; Sablayrolles, A.; and Jégou, H. 2021. Training data-efficient image transformers & distillation through attention. In *International Conference on Machine Learning*, 10347–10357. PMLR.
- Vaswani, A.; Shazeer, N.; Parmar, N.; Uszkoreit, J.; Jones, L.; Gomez, A. N.; Kaiser, Ł.; and Polosukhin, I. 2017. Attention is all you need. In *Advances in neural information processing systems*, 5998–6008.
- Wang, Q.; Yuan, Z.; Du, Q.; and Li, X. 2018. GETNET: A General End-to-End 2-D CNN Framework for Hyperspectral Image Change Detection. *IEEE Transactions on Geoscience and Remote Sensing*.
- Wang, R.; Ding, F.; Chen, J. W.; Liu, B.; and Jiao, L. 2020. SAR Image Change Detection Method via a Pyramid Pooling Convolutional Neural Network. In *IGARSS 2020 - 2020 IEEE International Geoscience and Remote Sensing Symposium*.
- Xie, E.; Wang, W.; Yu, Z.; Anandkumar, A.; Alvarez, J. M.; and Luo, P. 2021. SegFormer: Simple and Efficient Design for Semantic Segmentation with Transformers. *arXiv preprint arXiv:2105.15203*.
- Zhang, C.; Yue, P.; Tapete, D.; Jiang, L.; Shangguan, B.; Huang, L.; and Liu, G. 2020. A deeply supervised image fusion network for change detection in high resolution bi-temporal remote sensing images. *ISPRS Journal of Photogrammetry and Remote Sensing*, 166: 183–200.
- Zhang, L.; Hu, X.; Zhang, M.; Shu, Z.; and Zhou, H. 2021. Object-level change detection with a dual correlation attention-guided detector. *ISPRS Journal of Photogrammetry and Remote Sensing*, 177: 147–160.
- Zhang, M.; and Shi, W. 2020. A Feature Difference Convolutional Neural Network-Based Change Detection Method. *IEEE Transactions on Geoscience and Remote Sensing*, PP(99): 1–15.
- Zhao, J.-X.; Cao, Y.; Fan, D.-P.; Cheng, M.-M.; Li, X.-Y.; and Zhang, L. 2019. Contrast prior and fluid pyramid integration for RGBD salient object detection. In *Proceedings of the IEEE/CVF Conference on Computer Vision and Pattern Recognition*, 3927–3936.
- Zheng, S.; Lu, J.; Zhao, H.; Zhu, X.; Luo, Z.; Wang, Y.; Fu, Y.; Feng, J.; Xiang, T.; Torr, P. H.; et al. 2021. Rethinking semantic segmentation from a sequence-to-sequence perspective with transformers. In *Proceedings of the IEEE/CVF Conference on Computer Vision and Pattern Recognition*, 6881–6890.
- Zhu, X.; Su, W.; Lu, L.; Li, B.; Wang, X.; and Dai, J. 2020. Deformable detr: Deformable transformers for end-to-end object detection. *arXiv preprint arXiv:2010.04159*.